



HAL
open science

Evaluation of Conductive Porous Biobased Composites with Tunable Mechanical Properties for Potential Biological Applications

Laria Rodríguez-Quesada, Karla Ramírez-Sánchez, Cécile Formosa-Dague, Etienne Dague, Giovanni Sáenz-Arce, Carlos García-González, Fabián Vásquez-Sancho, Esteban Avendaño-Soto, Ricardo Starbird-Pérez

► To cite this version:

Laria Rodríguez-Quesada, Karla Ramírez-Sánchez, Cécile Formosa-Dague, Etienne Dague, Giovanni Sáenz-Arce, et al.. Evaluation of Conductive Porous Biobased Composites with Tunable Mechanical Properties for Potential Biological Applications. ACS Omega, 2024, 9 (43), pp.43426-43437. 10.1021/acsomega.4c04391 . hal-04750246

HAL Id: hal-04750246

<https://hal.science/hal-04750246v1>

Submitted on 23 Oct 2024

HAL is a multi-disciplinary open access archive for the deposit and dissemination of scientific research documents, whether they are published or not. The documents may come from teaching and research institutions in France or abroad, or from public or private research centers.

L'archive ouverte pluridisciplinaire **HAL**, est destinée au dépôt et à la diffusion de documents scientifiques de niveau recherche, publiés ou non, émanant des établissements d'enseignement et de recherche français ou étrangers, des laboratoires publics ou privés.

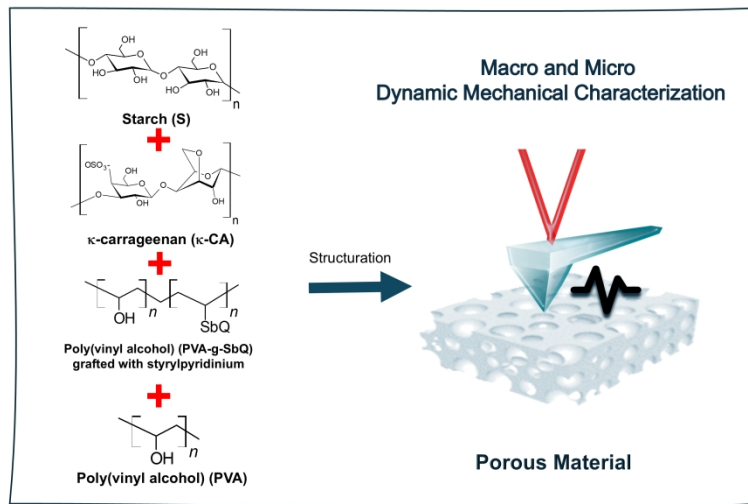
This document is confidential and is proprietary to the American Chemical Society and its authors. Do not copy or disclose without written permission. If you have received this item in error, notify the sender and delete all copies.

Evaluation of conductive porous biobased composites with tunable mechanical properties for potential biological applications

| | |
|-------------------------------|--|
| Journal: | ACS Omega |
| Manuscript ID | ao-2024-04391m.R3 |
| Manuscript Type: | Article |
| Date Submitted by the Author: | 30-Sep-2024 |
| Complete List of Authors: | <p>Rodríguez Quesada, Laria Fabiola; Instituto Tecnológico de Costa Rica, Centro de Investigación en Servicios Químicos y Microbiológicos (CEQIATEC), Escuela de Química; Instituto Tecnológico de Costa Rica, Master Program in Medical Devices Engineering; Universidad Nacional de Costa Rica, Departamento de Física, Facultad de Ciencias Exactas y Naturales</p> <p>Ramírez-Sánchez, Karla; Instituto Tecnológico de Costa Rica, Centro de Investigación en Servicios Químicos y Microbiológicos (CEQIATEC), Escuela de Química</p> <p>Formosa-Dague, Cécile; INSA Toulouse, TBI</p> <p>Dague, Etienne; Laboratoire d'analyse et d'architecture des systèmes, NanoBioSystem</p> <p>Sáenz-Arce, Giovanni; Universidad Nacional de Costa Rica, Physics; Universidad de Murcia, Centro de Investigación en Óptica y Nanofísica, Departamento de Física</p> <p>García-González, Carlos A.; Universidad de Santiago de Compostela, Departamento de Farmacia y Tecnología Farmacéutica, Facultad de Farmacia</p> <p>Vasquez-Sancho, Fabián; Universidad de Costa Rica, Centro de Investigación en Ciencia e Ingeniería de Materiales (CICIMA); Universidad de Costa Rica, School of Physics</p> <p>Avendaño-Soto, Esteban; Universidad de Costa Rica, Centro de Investigación en Ciencia e Ingeniería de Materiales (CICIMA); Universidad de Costa Rica, School of Physics</p> <p>Starbird-Perez, Ricardo; Instituto Tecnológico de Costa Rica, Centro de Investigación en Servicios Químicos y Microbiológicos (CEQIATEC), Escuela de Química</p> |

SCHOLARONE™
Manuscripts

1
2
3
4
5
6
7
8
9
10
11
12
13
14
15
16
17
18
19
20
21
22
23
24
25
26
27
28
29
30
31
32
33
34
35
36
37
38
39
40
41
42
43
44
45
46
47
48
49
50
51
52
53
54
55
56
57
58
59
60



338x190mm (300 x 300 DPI)

Evaluation of conductive porous biobased composites with tunable mechanical properties for potential biological applications

Laria Rodríguez-Quesada^{1,2,5*}, Karla Ramírez-Sánchez², Cécile Formosa-Dague³, Etienne Dague⁴, Giovanni Sáenz-Arce^{5,6}, Carlos A. García Gonzalez⁷, Fabián Vásquez-Sancho^{8,9}, Esteban Avendaño-Soto^{8,9} and Ricardo Starbird-Perez¹

¹Centro de Investigación en Servicios Químicos y Microbiológicos (CEQIATEC), Escuela de Química, Instituto Tecnológico de Costa Rica, Cartago 159-7050, Costa Rica.

²Master Program in Medical Devices Engineering, Instituto Tecnológico de Costa Rica, Cartago 159-7050, Costa Rica.

³TBI, Université de Toulouse, INSA, INRAE, CNRS, 31400 Toulouse, France.

⁴LAAS-CNRS, Université de Toulouse, CNRS, Toulouse, France.

⁵Departamento de Física, Facultad de Ciencias Exactas y Naturales, Universidad Nacional, Heredia 86-3000, Costa Rica.

⁶Centro de Investigación en Óptica y Nanofísica, Departamento de Física, Universidad de Murcia, 30100 Murcia, Spain

⁷Departamento de Farmacia y Tecnología Farmacéutica, Facultad de Farmacia, Universidad de Santiago de Compostela, 15782 Santiago de Compostela, Spain

⁸Centro de Investigación en Ciencia e Ingeniería de Materiales (CICIMA), Universidad de Costa Rica, San José 11501-2060, Costa Rica.

⁹School of Physics, Universidad de Costa Rica, San José 11501-2060, Costa Rica.

Corresponding author: larodriguez@itcr.ac.cr

Abstract

In this work, starch-based porous cryogels with controlled mechanical and electrical properties were prepared for tissue engineering applications. The starch cryogels were formulated using κ -carrageenan, polyvinyl alcohol (PVA) and styrylpyridinium-substituted PVA (SbQ) into the composite. A conductive cryogel was polymerized by chemical oxidation of 3,4-ethylenedioxythiophene (EDOT) using iron(III) p-toluenesulfonate as a strategy to control the electrical properties. The physical, thermal, and mechanical properties were evaluated for the obtained composites. Macro- and nanoscale results confirmed the capability of tuning the mechanical properties of the material by the addition of biopolymers in different contents. The presence of κ -carrageenan significantly increased the storage modulus and decreased the damping effect in the formulations. The presence of PVA showed a plasticizing effect in the formulations confirmed by the buffering effect and an increase in storage modulus. PVA-SBQ improved mechanical properties by cross-linking. The addition of PEDOT increased the mechanical behavior and electrical properties of the obtained materials.

Keywords: mechanical properties, cryogels, conductive composites, porous materials.

1. Introduction

In recent years, the modelling of the mechanical properties of 3D scaffolds for tissue engineering has become a challenge to provide a suitable environment to convey interactions between cells and the extracellular matrix (ECM) for growth, differentiation, and morphogenesis [1–3]. Synthetic extracellular matrices must possess similar biochemical and biophysical conditions as native tissues to allow proper proliferation and functionality [4]. Biophysical factors are important because, contrarily to biochemical factors, they have a longer lifetime and can be easily adjusted depending on the specific needs of the target tissue by adjusting the biomaterials composition [5].

Aiming the development of scaffolds with optimal nanomechanical and electrical properties is critical for advancing tissue engineering and for improving tissue replacement therapies in the future [6]. The ECM acts as a buffer for extra and intracellularly generated applied forces, which can have broad effects on cell function [7]. Mechanical interactions mediated by adhesion to the ECM and cell–cell junctions play a key part in transmitting forces that regulate intracellular signaling pathways [8]. Cells exert intrinsic forces on their environment through various mechanisms, including actomyosin contractility and cytoskeletal assembly. Cell-extrinsic shear, tensile and compressive forces can be applied to stem cells from external loads [9,10]. These forces are generated across different magnitudes and length scales (intracellular or external loads) [11–14]. Specifically, *in vitro* mechanical stimulation of mesenchymal stem cells (MSCs) has showed that tensile strain enhances osteogenesis and ethnogenesis but inhibits adipogenesis [15,16], whereas hydrostatic pressure and compressive loading induce chondrogenesis, and fluid flow-induced shear stress upregulates genes is associated to osteogenesis [17]. Biological frequency-dependent processes such as locomotion, respiration, and circulation are generated in the range between 0.1 and 1 Hz, so studies on ECM have shown that oscillatory mechanical stimulation within this frequency range can inhibit or induce differentiation of stem cells into desired lineages [10,18].

The cellular environment generates electrical stimuli by forces that alter the ECM-cell response. Cells in biological tissues are constantly exposed to endogenous electrical signals, for instance those generated in the nervous system [19,20] that

1
2
3 influences key processes, such as cell migration, proliferation, differentiation, and
4 growth factor production, which are essential for tissue formation and regeneration
5 [6,20]. Therefore, scaffolds may incorporate electrical characteristics, such as
6 electrical conductivity and electrical stimulation capability, to promote cell growth
7 and functionality.
8
9

10
11 The response to mechanical factors at different scales in synthetic extracellular
12 matrices have been evaluated by diverse techniques [21–24]. For instance, dynamic
13 compressive testing is a conventional method used to characterize the mechanical
14 bulk properties of a scaffold in the frequency range [21], while cellular interaction
15 and effects and electrical response can be evaluated by atomic force microscopy
16 (AFM) at conditions of the cellular microenvironment. Appropriate understanding
17 of these properties enables the creation of scaffolds that more closely mimic the
18 natural tissue environment, resulting in the generation of functional artificial tissues
19 and the promotion of tissue regeneration [25–27].
20
21

22
23 The formulation of ECM materials has an impact on the generated
24 mechanical/electrical response. Certain biocompatible [28] and biodegradable [29]
25 biopolymers (e.g. polysaccharides) have very similar properties to the native
26 macromolecules in the extracellular environment [30]. They may reduce the
27 promotion of chronic inflammation or immunological reactions and toxicity which
28 frequently occur when a synthetic polymer device is implanted into the host [31,32].
29 Composite formulation based on polysaccharides has the potential to tune the
30 polymeric device physical, mechanical and electrical properties for specific
31 biological applications. The mechanical and other physical properties of
32 polysaccharide-based polymers can be improved through the addition of other
33 biocompatibility polymers and percentage control such as polyvinyl alcohol (PVA)
34 and PVA-SbQ (Styrylpyridinium) [33,34]. These formulations may improve the
35 flexibility, strength, and chemical resistance due to the hydrogen bonding among
36 both macromolecules [33], allowing porous structures to be obtained [35], chemical
37 resistance and physical properties [36,37]. The SbQ group can undergo cross-linking
38 reaction under irradiation [38–40], modifying its properties such as water stability
39 and good storage stability [40]. Finally, the electrical properties are modulated by
40 the chemical deposition conductive polymer as a poly(3,4-ethylenedioxythiophene)
41 (PEDOT), which can provide the mechanical and electrical properties required for
42 generating stimuli-responsive smart biopolymers used in the field of tissue
43 engineering [41]. In this work, the mechanical and electrical properties of biobased-
44
45
46
47
48
49
50
51
52
53
54
55
56
57
58
59
60

1
2
3 modified scaffolds were tuned with varying composition of the evaluation and
4 critically evaluated for specific tissue requirements. The electrical properties were
5 modulated by the formulation and chemical deposition of the conductive polymer
6 as a poly(3,4-ethylenedioxythiophene) PEDOT, which can provide the mechanical
7 and electrical properties required for generated stimuli-responsive smart
8 biopolymers used in the field of tissue engineering applications.
9
10
11
12
13

14 **2. Materials and Methods**

15 *2.1. Materials and reagents*

16
17 The starch from corn (27% amylose content, quality level 200), κ -carrageenan (κ Ca)
18 from red algae (quality level 200), poly(vinyl alcohol) (PVA, quality level 200, Mw
19 89000-98000), 3,4-ethylenedioxythiophene (EDOT, 97% purity), iron(III) p-
20 toluenesulfonate hexahydrate (quality level 100), 2-Propanol (IPA, ACS reagent,
21 quality level 300) were purchased from Sigma-Aldrich (San José, Costa Rica).
22 Poly(vinyl alcohol) N-methyl-4(4'-formylstyryl) pyridinium methosulfate acetal
23 (PVA-SbQ) (Mw \approx 45000 g/mol; 13.3 % solution in water, 4.1 mol% SbQ) was
24 purchased from Polysciences (Warrington, Pennsylvania, United States of America).
25 Deionized water was used in all experiments.
26
27
28
29
30
31
32
33

34 *2.2. Starch cryogels preparation*

35
36 Polysaccharide-based cryogels were prepared from starch-based and κ Ca aqueous
37 solutions by continuous magnetic stirring (MS7-H550-S, DLAB, Beijing, China) at 300
38 rpm for 2 h or until homogeneous dissolution was observed, at room temperature.
39 Subsequently, a part of the starch was replaced by different concentrations of
40 poly(vinyl alcohol) and PVA substituted with styrylpyridinium groups (PVA-SbQ).
41 Thus, the total polymer concentration in the final formulation was always 9.5%
42 (expressed as a weight percentage of the initial mixing solution for cryogel
43 formation). The distribution of the concentrations per formulation can be seen in
44 Table 1.
45
46
47
48
49

50 Each formulation was autoclaved at 110 °C and 1.1 bar for 5 min (Tomin 322, Tomin
51 Medical equipment, New Taipei, Taiwan). The resulting viscous solution was
52 poured into cylindrical polyethylene molds of 1.2 cm diameter and 2 cm height.
53 They were stored at 4 °C for 4 days for starch retrogradation. The resulting
54
55
56
57
58
59
60

hydrogels were frozen at -20 °C for 48 h [42] and then freeze-dried for 24 h using a Labconco benchtop freeze dryer at -50 °C collector temperature and 0.050 mbar (FreeZone 2.5 Liter Benchtop Freeze Dryer, Kansas, EE. UU.). Cryogels with containing SbQ(St/ κ Ca/PVA-SbQ 0.1 and St/ κ Ca/PVA-SbQ 0.5), were gamma irradiated using 25 kGy (Ob-Servo Ignis, Izotop, Budapest, Hungary) to induce SbQ photo-reticulation.

Table 1: Composition of polysaccharide-based cryogel formulations.

| Formulation | Polymer content per formulation (wt. %) | | | |
|-----------------------------|--|-------------|------|---------|
| | St | κ Ca | PVA | PVA-SbQ |
| St | 9.00 | 0.00 | 0.00 | 0.00 |
| St/ κ Ca | 9.00 | 0.50 | 0.00 | 0.00 |
| St/ κ Ca/PVA 0.25 | 8.75 | 0.50 | 0.25 | 0.00 |
| St/ κ Ca/PVA 0.5 | 8.50 | 0.50 | 0.50 | 0.00 |
| St/ κ Ca/PVA 1.0 | 8.00 | 0.50 | 1.00 | 0.00 |
| St/ κ Ca/PVA 1.8 | 7.20 | 0.50 | 1.80 | 0.00 |
| St/ κ Ca/PVA-SbQ 0.1 | 8.00 | 0.50 | 0.90 | 0.10 |
| St/ κ Ca/PVA-SbQ 0.5 | 8.00 | 0.50 | 0.50 | 0.50 |

2.3. PEDOT-Starch polymerization

PEDOT was synthesized via oxidative chemical polymerization of EDOT onto the starch cryogel scaffold, adapted from previous works [43,44]. The starch cryogel sample was placed in an alcoholic solution containing isopropanol (IPA) and iron(III) p-toluenesulfonate hexahydrate 0.3 M [44]. The synthesis of PEDOT was performed by immersing the starch cryogel in iron(III) solution for 48 h [44]. The resulting scaffold was dried for 24 h in a vacuum oven (ADP 200C, Yamato-Scientific, Tokyo, Japan) at 45 °C and 85 kPa.

2.3.1 Physical characterization of polysaccharide-based cryogels.

Skeletal density of polysaccharide-based cryogels (ρ_{skel}) was determined using a nitrogen pycnometer (Ultrapyc 5000, Anton Paar Graz, Austria) set at room temperature (25 °C) and 19 psi, 20 replicates were used in the analysis (standard

1
2
3 deviation <2%). Cryogels bulk density (ρ_{bulk}) was calculated by weighing and
4 measuring individual cryogels dimensions. Finally, equation 1 and equation 2 were
5 used to calculate overall percentage porosity (ε) and total pore volume (V_p) of the
6 cryogels [45].
7
8
9

$$\varepsilon = 1 - \frac{\rho_{bulk}}{\rho_{skel}} \times 100 \quad (\text{equation 1})$$

$$V_p = \frac{1}{\rho_{bulk}} - \frac{1}{\rho_{skel}} \quad (\text{equation 2})$$

10
11
12
13
14
15
16
17
18 The relative volume of the samples is given as shrinkage percentage, and it was
19 obtained directly from geometric measurements of the samples before and after
20 freeze-drying process. Micrographs of the obtained cryogels were recorded by
21 scanning electron microscopy (JSM-IT500 InTouch Scope; JEOL, Tokyo, Japan).
22 Finally, the formulation of the samples was evaluated using the thermogravimetric
23 TGA/DTG technique. The samples were analyzed under an N₂ atmosphere with a
24 gas flow rate of 50 mL·min⁻¹. The samples were scanned from room temperature to
25 800 °C at a heating rate of 20 °C·min⁻¹ using high-resolution 5500 TGA (TA
26 instruments, Waters, New Castle, EE. UU.). Only the biopolymers degradation
27 range (i.e. 200 to 300 °C) was considered for comparison purposes in the main data
28 processing.
29
30
31
32
33
34
35

36 2.5. Mechanical and electrical characterization of the porous materials

37
38 The mechanical dynamic response and stiffness of different formulated scaffolds
39 were determined before and after the conductive polymer deposition using DMA
40 and AFM techniques. Dynamic frequency tests were performed in the linear
41 viscoelastic range to determine the frequency dependence of the storage modulus,
42 loss modulus and damping factor for the cryogels formulation (St, St/ κ Ca,
43 St/ κ Ca/PVA and St/ κ Ca/PVA-SbQ) for biomedical applications in a range from 1 to
44 100 Hz.
45
46
47
48
49
50

51 2.5.1 Dynamic mechanical properties of cryogels

52
53
54 Dynamic mechanical measurements of the samples were carried out in the RS2-GA
55 instrument (Waters, New Castle, EE. UU.). The starch cryogels were placed directly
56
57
58
59
60

1
2
3 on the surface geometry in compression mode. A compression geometry of 11 mm
4 was used in cryogels with heights of 1 cm. The mechanical properties were then
5 measured over time until the storage modulus reached an equilibrium value. The
6 storage and loss modulus were recorded at 0.5% strain to 1 from 100 Hz and at room
7 temperature (25 °C). Prior to each measurement, the specimens were prestressed at
8 0.1 N. In all these experiments, each measurement was performed at least in
9 triplicate, from new sample preparations.
10
11
12
13

14 15 2.5.2 Determination of the nanomechanical properties of cryogels by Atomic Force 16 Microscopy 17 18 19

20 Nanomechanical properties of cryogels were recorded by AFM, in air and liquid
21 (culture medium) using a Nanowizard IV XP AFM (JPK-Bruker, Billerica, USA). The
22 data were obtained using colloidal probes, prepared following the procedure
23 described in [46]. Briefly, they were obtained by attaching a single silica microsphere
24 (5 µm in diameter, Bangs Laboratories) with a thin layer of UV-curable glue (NOA
25 63, Norland Edmund Optics) on triangular tipless cantilevers (MLCT-O10, Bruker
26 probes, nominal spring constant of 0.6 N·m⁻¹). These colloidal probes were then used
27 in force spectroscopy experiments to measure the mechanical properties of cryogel
28 samples, with an applied force kept lower than 10 nN. The duration of a typical
29 experiment was a few minutes, which guaranteed that no significant water
30 evaporation occurred over this time interval. The force curves acquired were then
31 analyzed using the Data Processing software (JPK-Bruker). Using these force curves,
32 the stiffness could also be determined, using the Hooke law, calculated from the
33 slope of the linear portion of the raw force curves according to equation 3 where s is
34 the experimentally accessible slope of the compliance region reached for sufficient
35 loading force and k is the cantilever spring constant.
36
37
38
39
40
41
42
43
44
45

$$46 \quad k_{sample} = k \times \left(\frac{s}{1-s} \right) \quad (equation\ 3)$$

47
48
49

50 The analyses were performed under conditions where for all samples, the same
51 indentation segment length from the curve was analyzed. For all experiments, the
52 cantilevers used were calibrated using the thermal noise method. For microrheology
53 measurements, the colloidal probe was used to apply a determined force of 10 nN
54
55
56
57
58
59
60

(initial indentation), before applying a sinusoidal excitation signal at a frequency of 1 Hz. During these measurements, in-phase and out-of-phase signals are detected, and further used to determine the shear modulus G^* using the following equation (4) where G' is the storage modulus, G'' is the loss modulus, i is the complex unit, ν the Poisson ratio (assumed to be 0.5), δ_0 the initial indentation, R the spherical colloidal probe radius (here of 2.5 μm), δ^* the sinusoidal indentation, and F^* the sinusoidal force.

$$G^* = G' + iG'' = \frac{1-\nu}{4\sqrt{R\delta_0}} \frac{F^*}{\delta^*} \quad (\text{equation 4})$$

From these measurements, the G' and G'' values were extracted from 70 curves for each sample, and $\tan(\delta)$ was calculated, which corresponds to the ratio of G'' over G' .

2.5.3 AFM imaging

For images of height, mechanical and electrical measurements AFM NX10 (Park Systems, Suwon, Korea) was used. PinPoint™ Nanomechanical Mode™ and PinPoint Conductive AFM (C-AFM) were used for the measurements. The TAP 300 tip (nominal elastic constant of 40 $\text{N}\cdot\text{m}^{-1}$; Budget Sensors) was used for topographic and mechanical measurements. The CDT-CONTR tip (nominal elastic constant of 0.5 $\text{N}\cdot\text{m}^{-1}$; Nanosensors) was used for conductive measurements.

3. Results and Discussion

3.1 Additive effects of PVA and PVA-SbQ on porosity

The mechanical parameters in ECM may be related to the network mesh size and porosity, and thus be used to construct a reliable multidimensional correlation matrix. Our results showed that cryogels presented low bulk densities (ρ_{bulk}) (0.08–0.12 $\text{g}\cdot\text{cm}^{-3}$) in line with a previous work that stated low density (0.07 – 0.16 $\text{g}\cdot\text{cm}^{-3}$) values for starch aerogels and cryogels [47]. The presence of κ -carrageenan, PVA and PVA-SbQ in the cryogel formulation did not have a significant impact on the porous morphology. In general, there are not differences on the physical properties among formulations (Table 2), which mainly depend on the processing conditions [47]. The

obtained porosity was between 92 and 94% in all cases, which are in the range of the requirements for synthetic scaffolds to be used for tissue engineering applications, typically higher than 80% [48].

Table 2: Textural properties of the polysaccharide-based cryogels prepared by freeze-drying conditions.

| Formulation | Volumetric shrinkage (%) | ρ_{bulk} ($\text{g}\cdot\text{cm}^{-3}$) | ρ_{skel} ($\text{g}\cdot\text{cm}^{-3}$) | E (%) | V_p (cm^3) |
|-----------------|--------------------------|--|--|------------------|-------------------------|
| St | 19.9 ± 8.6 | 0.08 ± 0.02 | 1.42 ± 0.05 | 94.15 ± 0.85 | 11.54 ± 1.94 |
| St/ κ Ca | 14.6 ± 2.8 | 0.09 ± 0.01 | 1.33 ± 0.03 | 92.92 ± 0.44 | 9.94 ± 0.69 |
| PVA 0.25 | 12.7 ± 6.7 | 0.11 ± 0.01 | 1.41 ± 0.05 | 92.56 ± 0.40 | 8.82 ± 0.52 |
| PVA 0.5 | 13.4 ± 3.1 | 0.11 ± 0.02 | 1.33 ± 0.03 | 91.86 ± 0.17 | 8.51 ± 0.20 |
| PVA 1.0 | 14.1 ± 4.2 | 0.12 ± 0.05 | 1.46 ± 0.09 | 92.12 ± 0.24 | 8.04 ± 0.27 |
| PVA 1.8 | 17.9 ± 3.2 | 0.10 ± 0.01 | 1.43 ± 0.06 | 92.68 ± 0.39 | 8.91 ± 0.55 |
| PVA-SbQ 0.1 | 15.8 ± 4.3 | 0.10 ± 0.01 | 1.40 ± 0.04 | 93.25 ± 0.31 | 9.85 ± 0.48 |
| PVA-SbQ 0.5 | 13.2 ± 6.5 | 0.10 ± 0.01 | 1.38 ± 0.04 | 92.65 ± 0.60 | 9.11 ± 0.79 |

The volumetric shrinkage of the samples was affected by the formulation, and it is known that this shrinkage is mainly caused by liquid-gas surface tension and liquid-solid adhesive forces [49,50]. In our case, the shrinkage values were below 20% for all cryogel formulations (Table 2), similar to those results previously reported for starch-based structures [49]. However, the samples containing PVA and PVA-SbQ in the formulations showed a reduced shrinkage values compared to pure starch cryogels, due to their hydrophilic nature [51] and SbQ group cross-linking after gamma irradiation.

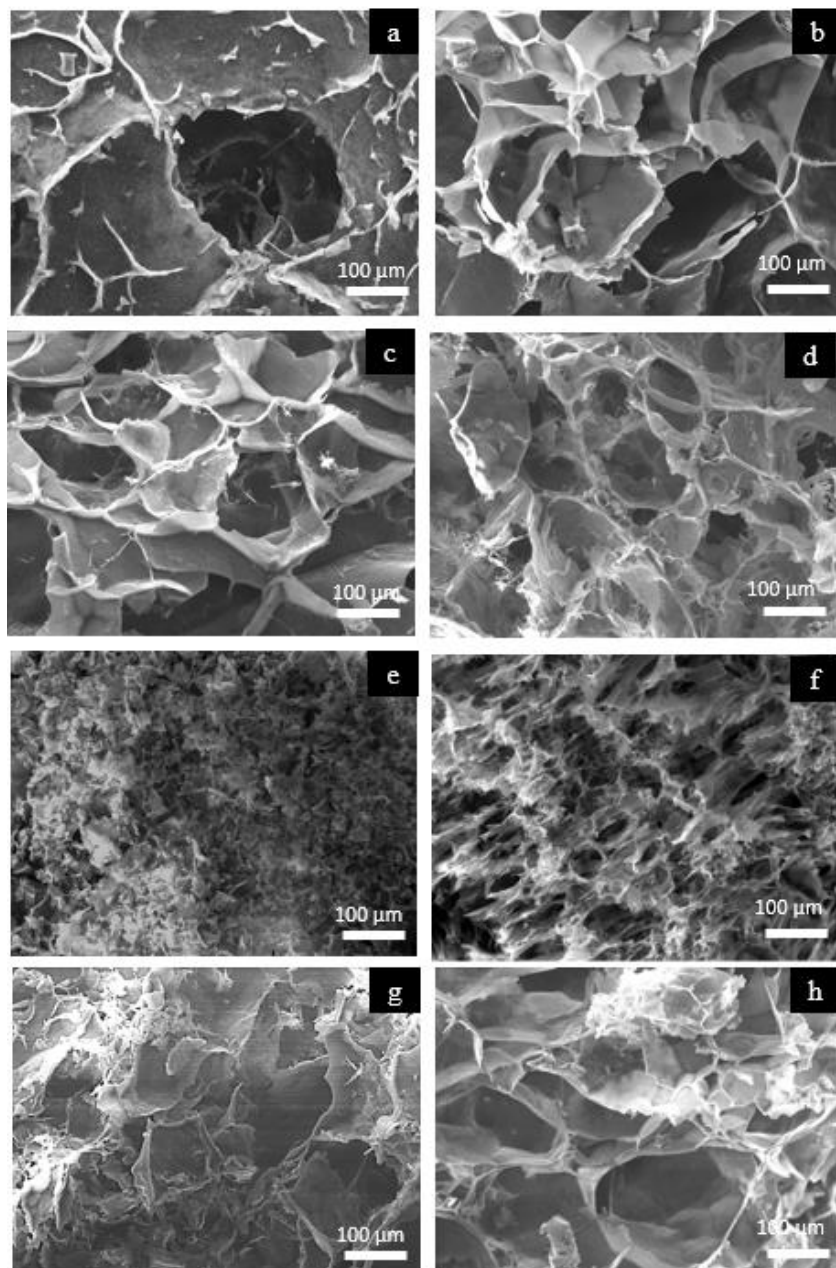
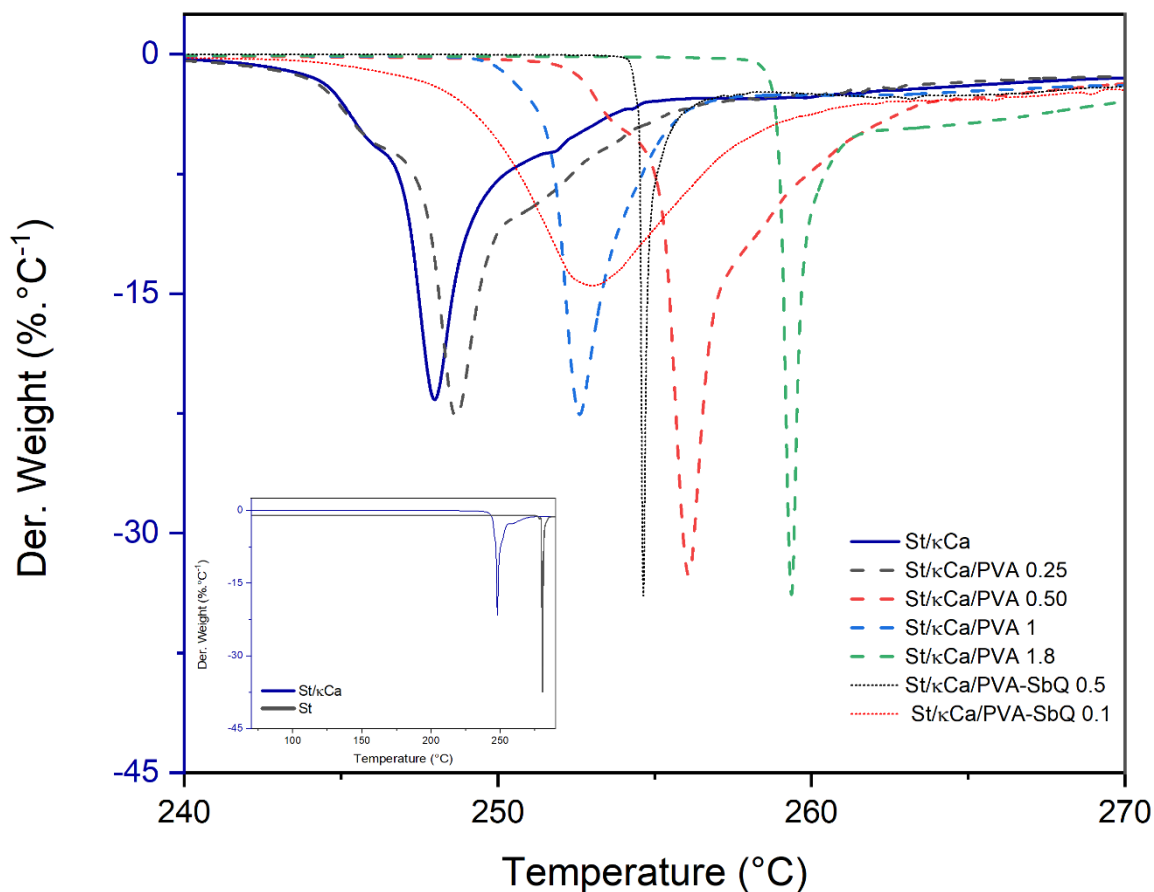


Figure 1. Macrostructure for different cryofractured porous materials: (a) St, (b) St/ κ Ca, (c) St/ κ Ca/PVA 0.25, (d) St/ κ Ca/PVA 0.5, (e) St/ κ Ca/PVA 1.0, (f) St/ κ Ca/PVA 1.8, (g) St/ κ Ca/PVA-SbQ 0.1 and (h) St/ κ Ca/PVA-SbQ 0.5.; obtained by SEM. Scale bar 100 μ m.

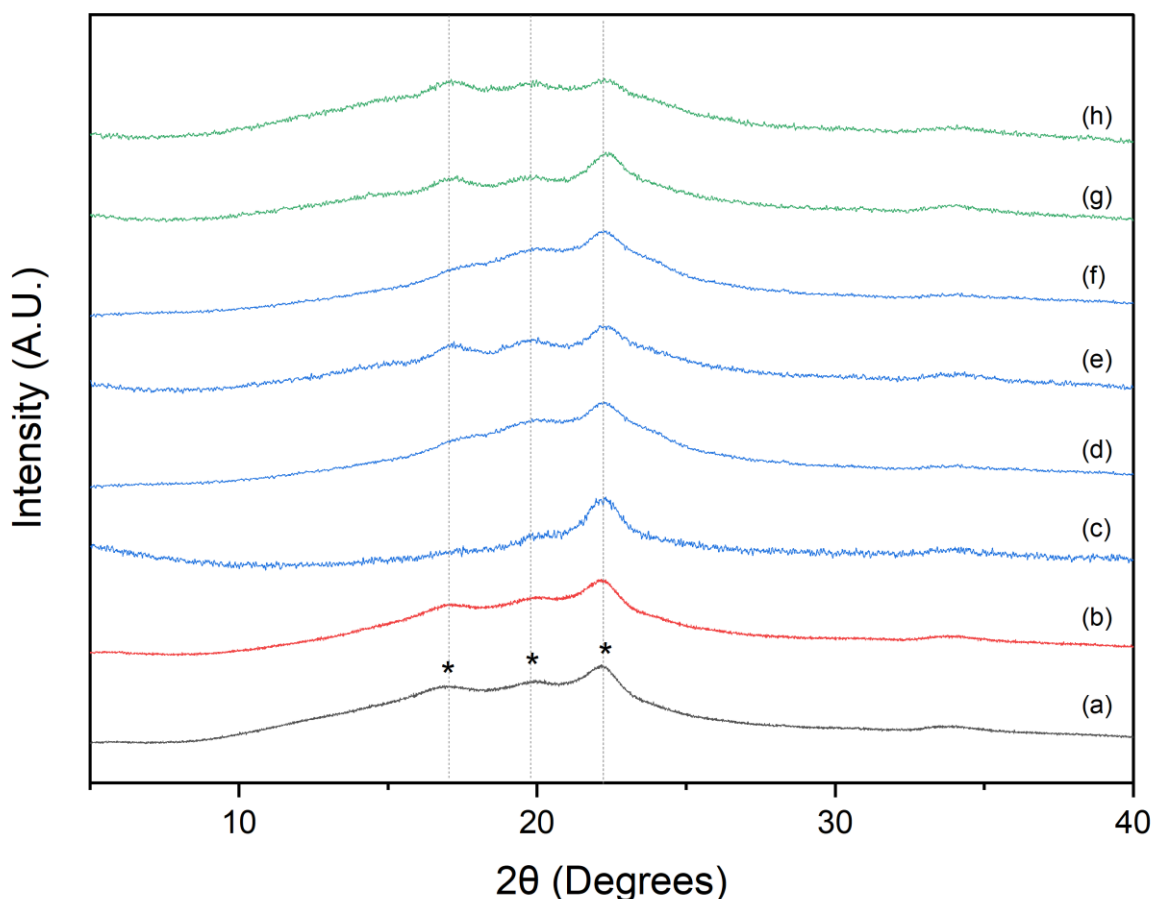
The inner structure of the cryogels was analyzed by SEM microscopy, preparing the sample by cryo-fracture. The presence of starch in the formulation had a strong

1
2
3 influence in the structural organization of the biomaterial and resembles the internal
4 solid open cell foam structure of similar starch porous materials [45,47]. The fracture
5 area in all cryogels showed to be dominated by crazing process (See Fig. 1 a-d). The
6 fracture area in all cryogels showed to be dominated by crazing process (See Fig. 1 a-d). The
7 presence of κ -carrageenan in the porous composites did not have an apparent
8 impact on the fracture area morphology [52]. However, PVA on the formulations
9 tends to change the fracture area at higher concentrations (i.e. 1.00 and 1.8 wt.%)
10 since the samples appear to have involved a mixed shear and crazing fracture
11 process (See Fig. 1e and f). This mixed behavior is not observed when PVA–SBQ is
12 incorporated in the formulations (See Fig. 1 g and h).



19
20
21
22
23
24
25
26
27
28
29
30
31
32
33
34
35
36
37
38
39
40
41
42
43
44
45
46
47
48
49
50 **Figure 2.** Derivate thermograms of porous materials in the degradation range. Inset:
51 Derivate comparative thermograms of the St and St/κCa.
52
53
54
55
56
57
58
59
60

1
2
3 TGA results in figure 2 showed that the starch template had a similar weight-loss
4 process as previously reported [43]. The main degradation stage is found at around
5 280 °C related to the polysaccharide degradation. The κ -carrageen in the starch
6 composite decrease the temperature degradation process, starting at ca. 248 °C. The
7 presence of PVA in the St/ κ Ca composites showed an increase in the thermal
8 stability along with the PVA amount (from 250 to 260°C) [53], but in all cases lower
9 than the porous starch. Larger amount of PVA in the formulation increase the initial
10 degradation temperature, due to the PVA thermal stability [34,54]. PVA-SBQ
11 molecule was included in the composite because its cross-linkable properties under
12 ionizing radiation. Therefore, a single degradation process at both concentrations,
13 confirmed the formation of a three-dimensional network in the composites [55].
14
15
16
17
18
19
20
21
22



52
53 **Figure 3.** XRD diffractograms of the porous materials: (a) St, (b) St/ κ Ca, (c)
54 St/ κ Ca/PVA 0.25, (d) St/ κ Ca/PVA 0.5, (e) St/ κ Ca/PVA 1.0, (f) St/ κ Ca/PVA 1.8, (g)
55 St/ κ Ca/PVA-SbQ 0.1 and (h) St/ κ Ca/PVA-SbQ 0.5.
56
57
58
59
60

1
2
3
4
5 XRD diffractograms (See Fig. 3) confirmed the presence of the crystalline starch
6 phase in all the formulations, with signals observed at $2\theta = 15.3^\circ$, 18.3° , and 23.1°
7 [44]. It has been stated that the crystalline regions, in the starch granule, are mainly
8 composed of the amylopectin short chains and the amorphous phase is composed
9 of its linear amylose component [53,54]. Additionally, it has been reported that the
10 starch crystalline phase during retrogradation experiments tends to steadily rise at
11 a lower rate than the amorphous phase [56]. So, our sample preparation conditions
12 allowed the crystallization of starch granules in all formulations, since no substantial
13 changes in the crystalline pattern were observed. Therefore, as no variations are
14 observed in the crystalline phase, and the thermal stability of the composites is
15 affected, it is expected that the κ Ca, PVA and SBQ molecules are embedded mainly
16 in the amorphous region.
17
18
19
20
21
22
23
24

25 *3.2 Macro mechanical response in the formulated cryogels*

26
27

28 *3.2.1 Effect of κ -carrageenan in the composite formulation*

29
30

31 The incorporation of κ -carrageenan in the cryogel caused an increase of 40% in the
32 elastic modulus of κ Ca (See Fig. 4), as previously reported using static compression
33 testing [52]. The interaction between starch and κ -carrageenan is not clear, since
34 different mechanisms may affect their mechanical behavior [52,57]. The mechanical
35 response in the composite depended on the carrageenan molecular weights and its
36 intrinsic viscosity, partial exclusion, or entrapment of carrageenan by swollen starch
37 granules [58]. Furthermore, during the cryogelation process, the phase transition of
38 κ -carrageenan solutions occurs because of the conformational transition from coiled-
39 coil to helix during cooling [57]. Further decrease in temperature results in
40 aggregation between ordered helices, possibly changing crystallization and thereby
41 increasing the mechanical properties of the cryogel [57].
42
43
44
45
46
47
48
49
50
51
52
53
54
55
56
57
58
59
60

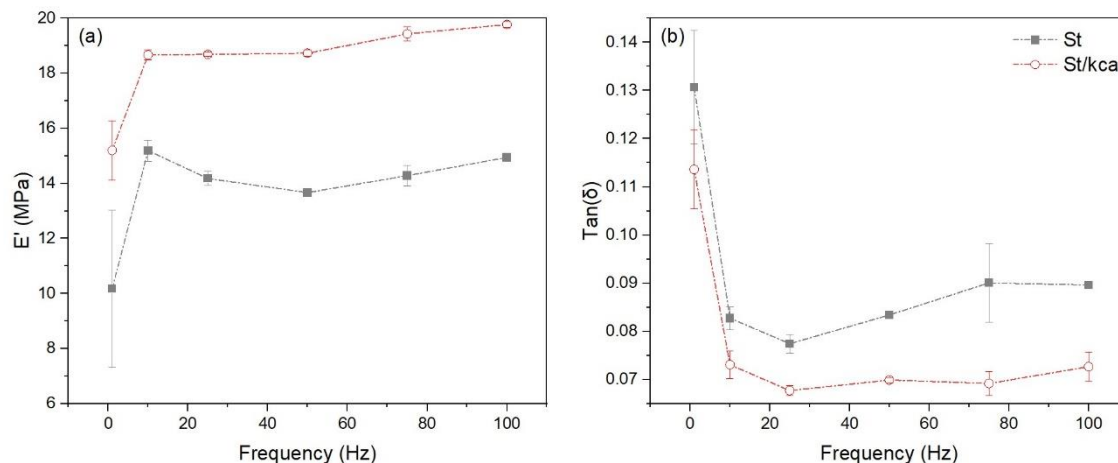


Figure 4. (a) Storage modulus (E') and (b) damping factor ($\text{Tan}(\delta)$) in starch template and St/ κ Ca cryogels measured by DMA testing in the range of frequencies (1–100 Hz).

3.2.2 Effect of polyvinyl alcohol (PVA) in the formulation

Regarding the PVA percentages in the starch cryogel template, the storage modulus of the cryogels followed a non-monotonic trend, from 16 MPa to 7 MPa (See. Fig. 5a). A decrease in the storage modulus, observed at low concentrations (i.e. St/ κ Ca/PVA 0.25, St/ κ Ca/PVA 0.5), suggested a plasticizing effect because starch and PVA are polar substances that have hydroxyl groups (OH single bond) in their chemical structure [10,59,60]. However, at high concentrations (i.e. St/ κ Ca/PVA 1.0, (f) St/ κ Ca/PVA 1.8), these highly polar hydroxyl groups tend to form intermolecular and intramolecular hydrogen bonds, consequently improving the integrity of the starch/PVA [61,62]. This behavior could be mainly due to the process used for the fabrication of the cryogels where it probably induces larger network interactions among polymers by the effect of the κ -carrageenan [63] or raising a rapid crystallization of amylose involving other molecules into single helices during cooling [64].

The damping effect ($\text{Tan}(\delta)$) (Fig 5b) did not register significant differences among the formulations with different percentages of PVA. However, it can be appreciated that formulations with PVA damping is higher than the St/ κ Ca cryogel. These data indicate that the viscous part of these structures is more prominent and dependent

on PVA effect in the composite. Thus, PVA provides matrices with more capacity of dissipating energy in the form of heat during a loading and unloading cycle of each of the formulations [4], confirming the plasticizing effect of PVA [59].

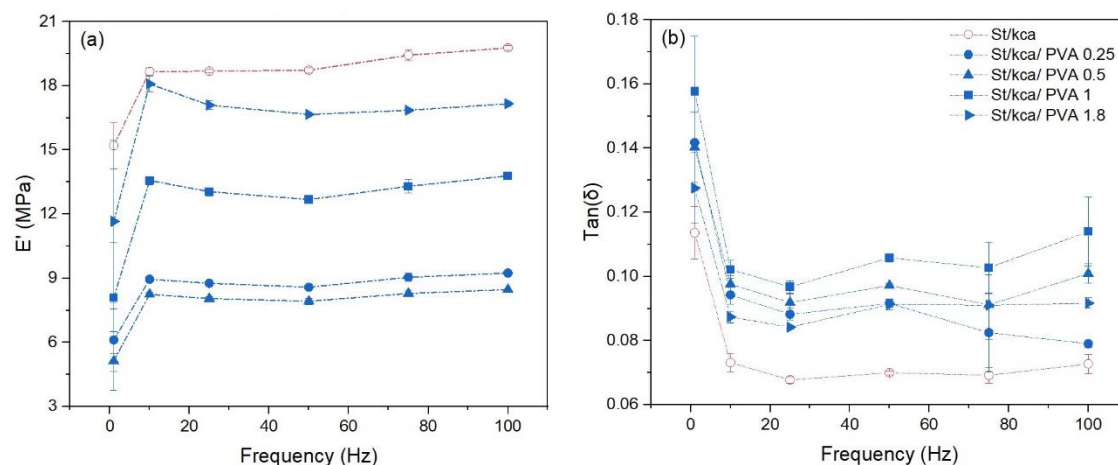


Figure 5. (a) Storage modulus (E') and (b) damping factor ($\tan(\delta)$) curves in St/κCa and St/PVA cryogels measured by DMA testing in 1–100 Hz range of frequencies.

3.2.3 Effect of Polyvinyl alcohol- Styrylpyridinium (PVA-SbQ) in the formulation

In Figure 6, a trend is observed for the St/κCa/PVA-SbQ composites at different PVA-SbQ concentrations. These results suggest that enhancement in structural entanglement increases the storage modulus [65], barely affecting the loss-modulus response. The relatively high storage modulus values may be caused by the crosslinked network created by the PVA-SbQ [38,39]. According to previous reports, an increase on the radiation promotes a chemical cross-linking as result of the SbQ molecules dimerization in the PVA-SbQ chains [37,39,66]. A molecular restraint caused by the crosslinked structure may increase the elastic phase (storage modulus). An improvement in storage can influence the scaffold's ability to dissipate energy and absorb impacts, which can be beneficial in protecting the muscle cells from excessive stresses and improve the structural support at the same time [3]. The resulting cryogels retain the ability to store elastic energy without large energy dissipations, characteristic of the PVA.

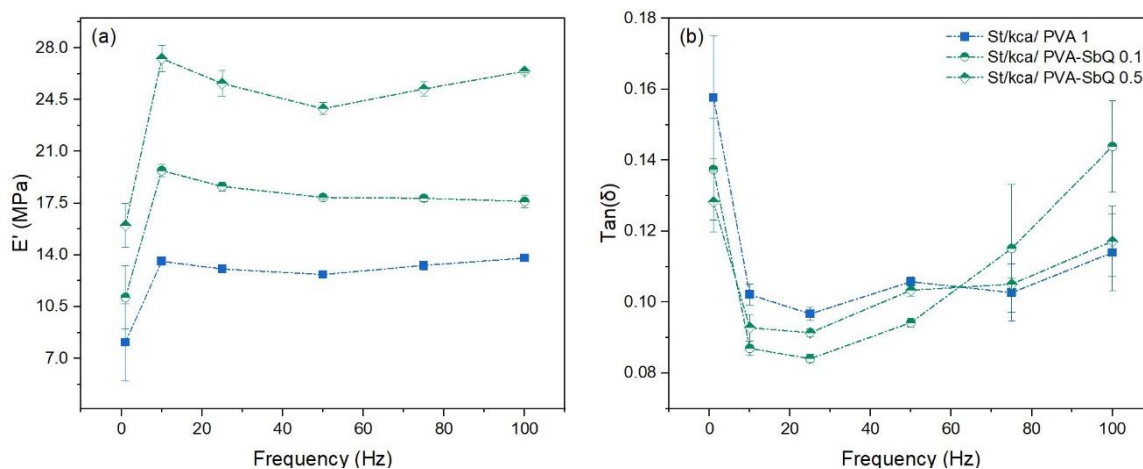


Figure 6. (a) Storage modulus (E') and (b) damping factor ($\text{Tan}(\delta)$) curves in St/PVA and St/PVA-SbQ cryogels measured by DMA testing in the 1–100 Hz range of frequencies.

3.2.4 Mechanical response of EDOT polymerization in the formulation

Storage modulus and viscous behavior of cryogels increased after the PEDOT polymerization on the cryogels (See. Fig. 7). According to the post-polymerization results, the changes in mechanical properties could be related to the interaction between κ -carrageenan and PEDOT. The improvement of the physicochemical and biological properties of PEDOT was associated with the presence of doping agents. Doping agents are substances that enable electrical conductivity in the polymer through the formation of strong charge-trapping centers (polaron and bipolaron) [67]. The κ -carrageenan is an interesting polysaccharide to investigate its potency as a dopant for PEDOT [52,68]. It can act as a doping agent since the sulfonate groups of κ -carrageenan can dope the conducting polymer through the interaction between sulfonate groups and EDOT groups [52,69]. According to previous reports, the κ -carrageenans may form double helix structures in the presence of cations through ionic interactions with sulfonate groups. The possible formed structure can promote aggregation to binding sites and cross-linking of the polysaccharide-cation system with the conducting polymer, thus generating an increase in the mechanical properties of the material [57].

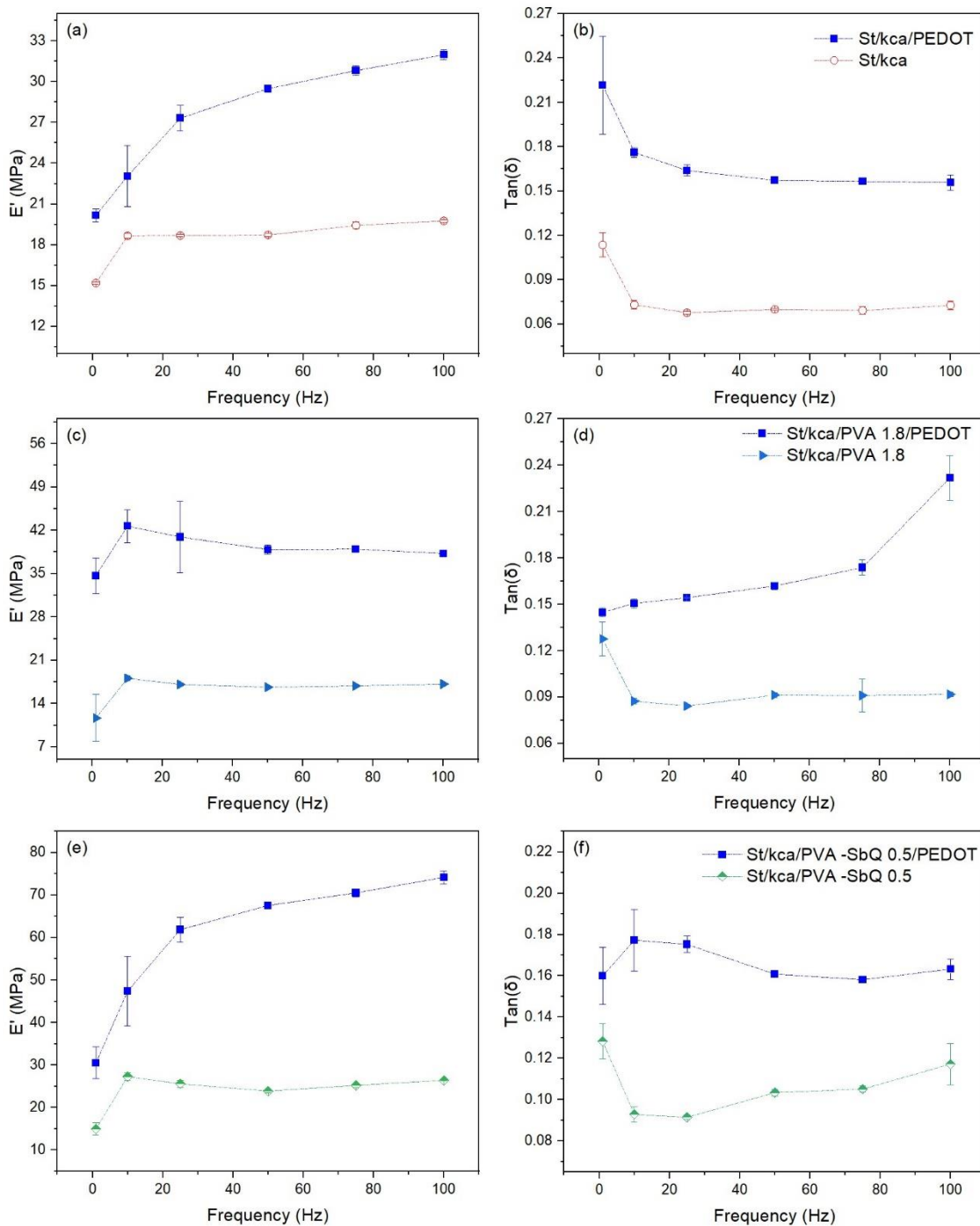


Figure 7. (a,c and e) Storage modulus (E') and (b, d and f) damping factor ($\text{Tan}(\delta)$) curves in polymerizates PEDOT cryogels measured by DMA testing in the 1–100 Hz range of frequencies.

3.4 Surface electrical and mechanical properties characterization of templates and PEDOT coated cryogels by Atomic Force Microscopy (AFM).

Considering the heterogeneity of the cryogel surface (See Fig. 8a), eight measurement areas on the surface of each formulation were randomly selected for characterization by AFM in electric mode. The electrical (See Fig 8b) and mechanical (See Fig 8c-d) properties of a polymerized cryogel were obtained. Although their porosity, qualitative analysis confirmed that the cryogel surface can conduct electricity at local scales and it is also possible to associate with its local mechanical response distributions.

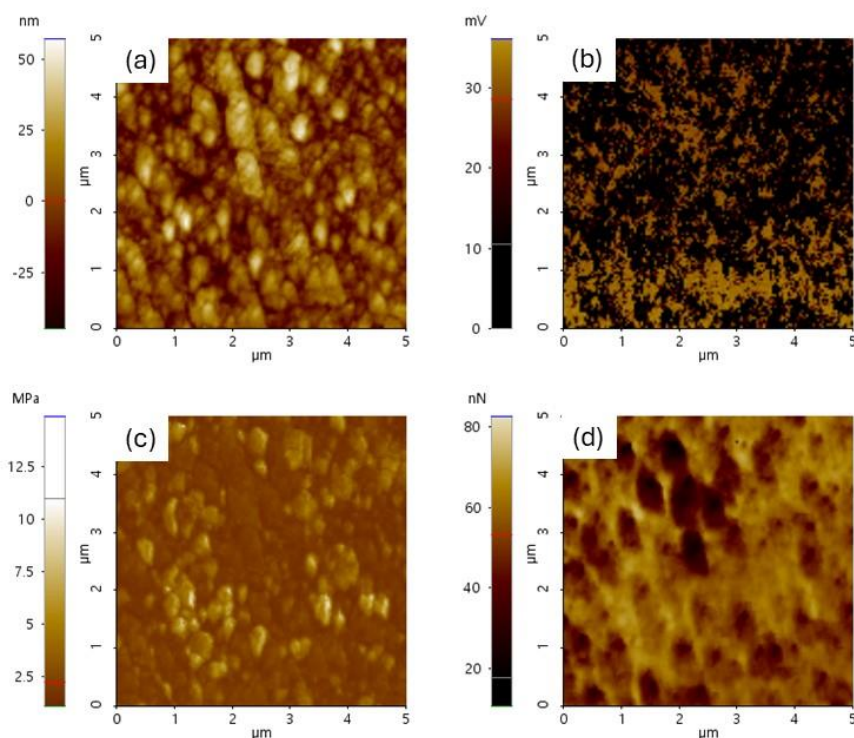


Figure 8. Mechanical and electrical behavior of the PEDOT cryogel: (a) topography, (b) current, (c) modulus and (d) adhesion response.

Biological and biochemical signals and the natural functions of cells and tissues are greatly affected by the physical properties of the microenvironment [5], for this reason, it is important to consider the effect of some of the fluids present on cell growth [70]. These physical factors are highly mixed in living tissues, which greatly complicates *in vivo* physical properties and affects synthetic matrices. Surface fluids

1
2
3 may alter the morphological integrity and mechanical response of the ECM as can
4 nutrient transport [71]. One way to assess local behavior in culture media is through
5 the appropriate use of atomic force microscopy tools. In this study, the AFM was
6 used to determine the local physical properties of the addition of formulations and
7 the influence of culture medium components on the mechanical properties and
8 integrity of cryogels for tissue engineering and bioengineering applications. In the
9 air study, the results showed a significant local increase with PVA response and a
10 decrease with the presence of SbQ.
11
12
13
14
15
16

17 The stiffness of the sample can be determined using AFM measurement, from the
18 slope of the force-separation curve in the contact region. The results obtained in the
19 culture medium showed that the immersion of the cryogels in the culture medium
20 had a significant impact on the composite stiffness, and their physical integrity as
21 shown in Figure 9. The trends of these results were compared with the stiffness
22 distribution in air, and they agree with those reported in Figure 8. In general, PEDOT
23 deposition on the cryogels increases the matrix resistance of them in a liquid
24 medium and improves the mechanicals properties of the matrix.
25
26
27
28
29
30
31
32
33
34
35
36
37
38
39
40
41
42
43
44
45
46
47
48
49
50
51
52
53
54
55
56
57
58
59
60

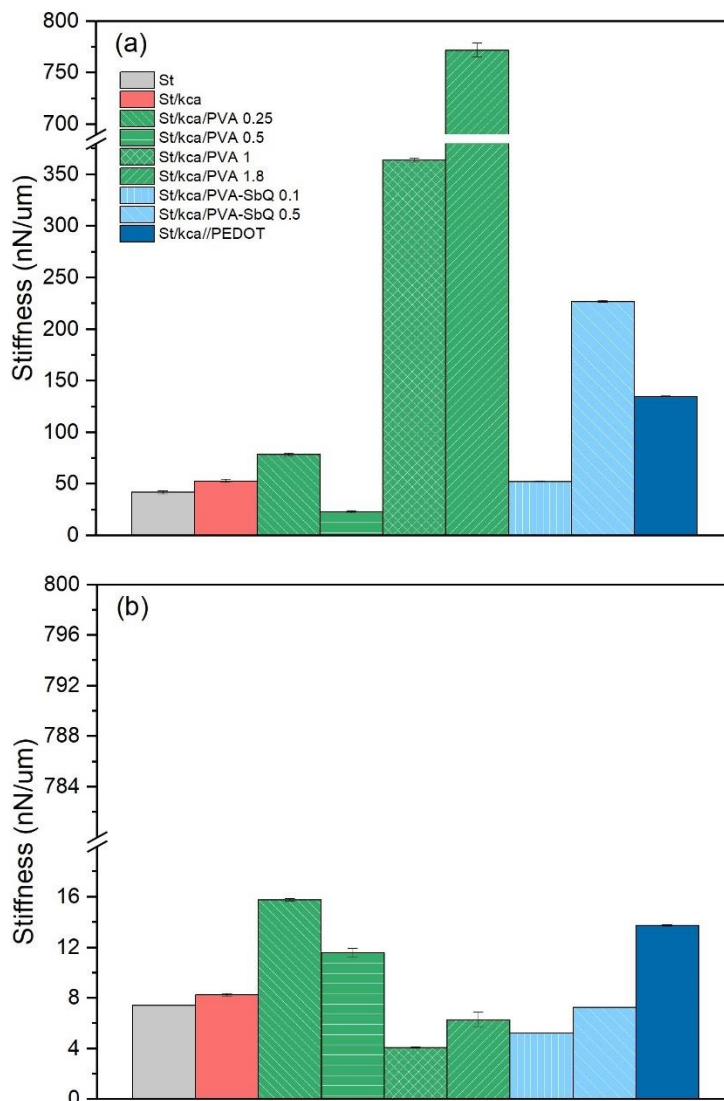


Figure 9. Local mechanical integrity in (a) air and (b) culture medium of different cryogel formulations measured by AFM testing.

Additionally, the nano-dynamic measurements carried out on the cryogels showed a heterogeneous mechanical response. In table 3 are summarized the average result of dynamic mechanical properties at nano and macro scale. The results show the same trend among formulations. It is observed that the storage and viscous capacity increase with the addition of PVA and SbQ. The composition of the formulations through adjusting small concentrations of PVA and PVA-SbQ, the mechanical properties such as viscoelasticity of the cryogel can be conveniently modulated to achieve the requirements for the specific application. Due to the sample complex

morphology, there are variations in the reported data for mechanical research at local and macro scale.

Table 3. Comparison of measurements of viscoelastic and young's modulus of components in porous material by AFM and DMA at 1 Hz.

| Formulation | AFM | | DMA | |
|-----------------------------|------------------|--------------------------------|------------------|--------------------------------|
| | Tan (δ) | Storage Modulus (<i>kPa</i>) | Tan (δ) | Storage Modulus (<i>MPa</i>) |
| St | 0.09 \pm 0.12 | 29 \pm 13 | 0.08 \pm 0.05 | 14.1 \pm 3.9 |
| St/ κ Ca | 0.19 \pm 0.23 | 219 \pm 125 | 0.11 \pm 0.12 | 19.6 \pm 1.7 |
| St/ κ Ca/PVA 0.25 | 0.06 \pm 0.05 | 22 \pm 26 | 0.11 \pm 0.15 | 24.3 \pm 3.7 |
| St/ κ Ca/PVA 0.5 | 0.07 \pm 0.03 | 20.6 \pm 5.4 | 0.09 \pm 0.04 | 10.2 \pm 1.4 |
| St/ κ Ca/PVA 1.0 | 0.12 \pm 0.11 | 14.5 \pm 4.3 | 0.12 \pm 0.23 | 17.8 \pm 4.3 |
| St/ κ Ca/PVA 1.8 | 0.13 \pm 0.22 | 1.51 \pm 1.6 | 0.14 \pm 0.12 | 17.5 \pm 4.3 |
| St/ κ Ca/PVA-SbQ 0.1 | 0.14 \pm 0.10 | 38.9 \pm 2.9 | 0.10 \pm 0.18 | 21.8 \pm 2.7 |
| St/ κ Ca/PVA-SbQ 0.5 | 0.08 \pm 0.54 | 45.0 \pm 3.3 | 0.07 \pm 0.05 | 23.7 \pm 2.7 |

A key challenge when characterizing the mechanical properties of synthetic ECM for tissues is to correlate information from conventional histological approaches with mechanical testing methods. Some reviewed the theories and analytical methods used to characterize the elastic properties of polymer gels and biological materials [72,73]. Although progress has been made in this area, they concluded that no model exists that can work as a universal constitutive law for soft elastic materials. The appropriate mechanical behavior may vary depending on the tissue and cell type [4], since certain cells may require a more elastic environment while others may benefit from higher viscosity. In other hand, the mechanical response value can be influenced by the type of geometries of deformation such as tensile, compression or shear test [23,74], the condition of the experiment used to take the mechanical property values, including the level of applied mechanical stress or strain, the rate of deformation, the geometry of the probe and the location probed in the material [23] and the elastic modulus range and length scale of the typical spatial resolution [26,72]. It is important to generate a general range of controllable mechanical properties in the synthetic ECM while providing mechanical support and structural stability to allow comparison with some similar theoretical reports with similar conditions and eventually perform cell-specific experiments.

1
2
3
4
5 In human bodies, the mechanical properties (the ratio of stress to strain referring to
6 the elasticity of materials) of tissues can vary by more than seven orders of
7 magnitude, as low as 167 Pa for brain tissue and as high as 5.4 GPa for cortical bone
8 [26]. The ECM stiffness (or measured as Young's Modulus) presents widely diverse
9 spanning from the brain (1–3 kPa) [75,76] to muscle (23–42 kPa) [77], blood vessel
10 (1.16–860 MPa) [27], tendon (136–820 MPa) [70], or bone (15–40 GPa) [78]. For the
11 cryogel formulations, the storage modulus-which represents the elastic part of the
12 complex modulus was like the published results for muscle and adipose tissue only
13 in the case of the St/ κ ca/PVA-SbQ formulation [8]. In the case of St/ κ ca/PVA 0.5
14 matrices, due to their highly viscous behavior, they could be more functional for
15 brain tissues. Conductive polymer deposition improved the storage capacities, so it
16 is possible to tune the electrical and mechanical properties of cryogels with lower
17 storage response to be functional in tissues with high elastic storage capacities, such
18 as muscle tissues.
19
20
21
22
23
24
25
26
27

28 **4. Conclusion**

29
30
31 Our results show a clear thermal and mechanical effect due to the polymers in the
32 formulation with a slight difference in the porosity and density among samples. The
33 mechanical behavior of the samples was studied at macro and nanoscale, confirming
34 that their properties have been tuned by adding biopolymers in the different
35 formulations. Specifically, κ -carrageenan, at 5 wt. %, significantly increase the
36 storage module and a decrease on the damping behavior effect in the formulations.
37 PVA showed a plasticize effect on the formulations confirmed by the damping effect
38 and an increase on the storage module along with PVA concentration (up to ca. 20
39 wt.%). Meanwhile, PVA-SBQ at low concentration (1 and 5 wt.%) enhanced the
40 mechanical properties through a cross-linking process along with its physical
41 stability. Finally, PEDOT on the composite showed an increase in the composite
42 mechanical behavior and improving their electrical response. The mechanical,
43 thermal, and physical behavior trend confirmed the potential modulation of the
44 porous material properties by the biopolymers in the formulation. Our results allow
45 the design of extracellular matrices for specific tissue engineering applications.
46
47
48
49
50
51
52
53
54
55
56
57
58
59
60

1
2
3 **Author Contributions:** Conceptualization, L.R.-Q. and R.S.-P.; methodology, L.R.-
4 Q., K.R.-S., C.F.-D., G.S.-A., F.V.-S., E.A.-S. and R.S.-P.; validation, L.R.-Q., C.F.-D.,
5 G.S.-A., F.V.-S. and R.S.-P.; formal analysis, L.R.-Q. and R.S.-P.; investigation, L.R.-
6 Q. and R.S.-P.; resources, K.R.-S. and R.S.-P.; data curation, L.R.-Q. .; writing and
7 original draft preparation, L.R.-Q., C.F.-D., G.S.-A., F.V.-S. and R.S.-P.; writing,
8 review, and editing, L.R.-Q., C.F.-D., E.D., G.S.-A., C.G.-G., F.V.-S., E.A.-S. and R.S.-
9 P.; visualization, L.R.-Q., C.F.-D., G.S.-A., F.V.-S., E.A.-S. and R.S.-P.; supervision,
10 R.S.-P.; project administration K.R.-S. and R.S.-P.; funding acquisition, R.S.-P. All
11 authors have read and agreed to the published version of the manuscript.
12
13
14
15
16
17
18

19 **Funding:** This research was funded by Vicerrectoría de Investigación from Instituto
20 Tecnológico de Costa Rica (VIE-ITCR), grant number FEES-1713023, and the
21 Ministerio de Ciencia, Tecnología y Telecomunicaciones de Costa Rica (MICITT),
22 grant number FI-038B-19. This work was funded by
23 MICIU/AEI/10.13039/501100011033 [grant PID2020-120010RB-I00] and ERDF/EU.
24
25
26
27

28 **Institutional Review Board Statement:** Not applicable.
29
30

31 **Informed Consent Statement:** Not applicable.
32
33

34 **Data Availability Statement:** The raw data of this study is available from the
35 corresponding authors (L.R.-Q. and R.S.-P) on request: larodriguez@itcr.ac.cr.
36
37
38

39 **Acknowledgments:** We would like to acknowledge Centro de Investigación en
40 Ciencia e Ingeniería de Materiales (CICIMA, Universidad de Costa Rica) and
41 Toulouse Biotechnology Institute (TBI) of the Institut National des Sciences
42 Appliquées (INSA, University of Toulouse) for their support in the sample
43 characterization. Laria Rodríguez-Quesada thank the Medical Devices Master
44 Program and the Postgraduate Office at TEC for the awarded scholarship during
45 this project. G.S.A. is supported by a María Zambrano contract of “Programa de
46 Ayudas para la Recualificación del Sistema Universitario Español”. Work carried
47 out in the framework of the ECO-AERoGELS COST Innovators Grant (ref. IG18125)
48 and funded by the European Commission. We would like to thank our reviewers
49 because their accurate observations helped us to improve our manuscript. RGSF-
50 RIP.
51
52
53
54
55
56
57
58
59
60

Conflicts of Interest: The authors declare no conflict of interest.

5. References

1. Jansen, K.A.; Atherton, P.; Ballestrem, C. Mechanotransduction at the Cell-Matrix Interface. *Semin Cell Dev Biol* 2017, *71*, 75–83.
2. Hastings, J.F.; Skhinas, J.N.; Fey, D.; Croucher, D.R.; Cox, T.R. The Extracellular Matrix as a Key Regulator of Intracellular Signalling Networks. *Br J Pharmacol* 2019, *176*, 82–92.
3. O'Brien, F.J. Biomaterials & Scaffolds for Tissue Engineering. *Materials Today* 2011, *14*, 88–95.
4. Xie, W.; Wei, X.; Kang, H.; Jiang, H.; Chu, Z.; Lin, Y.; Hou, Y.; Wei, Q. Static and Dynamic: Evolving Biomaterial Mechanical Properties to Control Cellular Mechanotransduction. *Advanced Science* 2023.
5. Li, J.; Liu, Y.; Zhang, Y.; Yao, B.; Enhejirigala, B.; Li, Z.; Song, W.; Wang, Y.; Duan, X.; Yuan, X.; et al. Biophysical and Biochemical Cues of Biomaterials Guide Mesenchymal Stem Cell Behaviors. *Front Cell Dev Biol* 2021, *9*.
6. Chen, C.; Bai, X.; Ding, Y.; Lee, I.S. Electrical Stimulation as a Novel Tool for Regulating Cell Behavior in Tissue Engineering. *Biomater Res* 2019, *23*.
7. Yamada, K.M.; Doyle, A.D.; Lu, J. Cell–3D Matrix Interactions: Recent Advances and Opportunities. *Trends Cell Biol* 2022, *32*, 883–895.
8. Chaudhuri, O.; Cooper-White, J.; Janmey, P.A.; Mooney, D.J.; Shenoy, V.B. Effects of Extracellular Matrix Viscoelasticity on Cellular Behaviour. *Nature* 2020, *584*, 535–546.
9. Wang, N.; Tytell, J.D.; Ingber, D. Mechanotransduction at a Distance: Mechanically Coupling the Extracellular Matrix with the Nucleus. *Nature* **2009**, *10*, 75–79, doi:10.1038/nrm2594.
10. Vining, K.H.; Mooney, D.J. Mechanical Forces Direct Stem Cell Behaviour in Development and Regeneration. *Nat Rev Mol Cell Biol* 2017, *18*, 728–742.
11. Zhang, W.; Kong, C.W.; Tong, M.H.; Chooi, W.H.; Huang, N.; Li, R.A.; Chan, B.P. Maturation of Human Embryonic Stem Cell-Derived Cardiomyocytes (HESC-CMs) in 3D Collagen Matrix: Effects of Niche Cell Supplementation and Mechanical Stimulation. *Acta Biomater* **2017**, *49*, 204–217, doi:10.1016/j.actbio.2016.11.058.
12. Valentin, J.E.; Turner, N.J.; Gilbert, T.W.; Badylak, S.F. Functional Skeletal Muscle Formation with a Biologic Scaffold. *Biomaterials* **2010**, *31*, 7475–7484, doi:10.1016/j.biomaterials.2010.06.039.
13. Park, S.H.; Park, S.A.; Kang, Y.G.; Shin, J.W.; Park, Y.S.; Gu, S.R.; Wu, Y.R.; Wei, J.; Shin, J.W. PCL/β-TCP Composite Scaffolds Exhibit Positive Osteogenic Differentiation with Mechanical Stimulation. *Tissue Eng Regen Med* **2017**, *14*, 349–358, doi:10.1007/s13770-017-0022-9.
14. Zöllner, A.M.; Abilez, O.J.; Böl, M.; Kuhl, E. Stretching Skeletal Muscle: Chronic Muscle Lengthening through Sarcomerogenesis. *PLoS One* **2012**, *7*, doi:10.1371/journal.pone.0045661.

15. Sen, B.; Xie, Z.; Case, N.; Ma, M.; Rubin, C.; Rubin, J. Mechanical Strain Inhibits Adipogenesis in Mesenchymal Stem Cells by Stimulating a Durable β -Catenin Signal. *Endocrinology* **2008**, *149*, 6065–6075, doi:10.1210/en.2008-0687.
16. Simmons, C.A.; Matlis, S.; Thornton, A.J.; Chen, S.; Wang, C.Y.; Mooney, D.J. Cyclic Strain Enhances Matrix Mineralization by Adult Human Mesenchymal Stem Cells via the Extracellular Signal-Regulated Kinase (ERK1/2) Signaling Pathway. *J Biomech* **2003**, *36*, 1087–1096, doi:10.1016/S0021-9290(03)00110-6.
17. Robin M, D.S.; Gwendolen C, R. Mesenchymal Stem Cell responses to Mechanical Stimuli. *Muscles, Ligaments and Tendons* **2012**, *2*, 169–180.
18. Moeendarbary, E.; Harris, A.R. Cell Mechanics: Principles, Practices, and Prospects. *Wiley Interdiscip Rev Syst Biol Med* **2014**, *6*, 371–388, doi:10.1002/wsbm.1275.
19. Rajabi, A.H.; Jaffe, M.; Arinzech, T.L. Piezoelectric Materials for Tissue Regeneration: A Review. *Acta Biomater* **2015**, *24*, 12–23.
20. Casella, A.; Panitch, A.; Leach, J.K. Endogenous Electric Signaling as a Blueprint for Conductive Materials in Tissue Engineering. *Bioelectricity* **2021**, *3*, 27–41.
21. Navindaran, K.; Kang, J.S.; Moon, K. Techniques for Characterizing Mechanical Properties of Soft Tissues. *J Mech Behav Biomed Mater* **2023**, *138*, 105575, doi:https://doi.org/10.1016/j.jmbbm.2022.105575.
22. Burnham, N.A.; Colton, R.J. Measuring the Nanomechanical Properties and Surface Forces of Materials Using an Atomic Force Microscope. *Journal of Vacuum Science & Technology A: Vacuum, Surfaces, and Films* **1989**, *7*, 2906–2913, doi:10.1116/1.576168.
23. Wu, P.H.; Aroush, D.R. Ben; Asnacios, A.; Chen, W.C.; Dokukin, M.E.; Doss, B.L.; Durand-Smet, P.; Ekpenyong, A.; Guck, J.; Guz, N. V.; et al. A Comparison of Methods to Assess Cell Mechanical Properties. *Nat Methods* **2018**, *15*, 491–498, doi:10.1038/s41592-018-0015-1.
24. Iglesias-Mejuto, A.; Magariños, B.; Ferreira-Gonçalves, T.; Starbird-Pérez, R.; Álvarez-Lorenzo, C.; Reis, C.P.; Ardao, I.; García-González, C.A. Vancomycin-Loaded Methylcellulose Aerogel Scaffolds for Advanced Bone Tissue Engineering. *Carbohydr Polym* **2024**, *324*, doi:10.1016/j.carbpol.2023.121536.
25. Leong, K.F.; Chua, C.K.; Sudarmadji, N.; Yeong, W.Y. Engineering Functionally Graded Tissue Engineering Scaffolds. *J Mech Behav Biomed Mater* **2008**, *1*, 140–152.
26. B., A.; Rao, S.; Pandya, H.J. Engineering Approaches for Characterizing Soft Tissue Mechanical Properties: A Review. *Clinical Biomechanics* **2019**, *69*, 127–140.
27. Dey, K.; Roca, E.; Ramorino, G.; Sartore, L. Progress in the Mechanical Modulation of Cell Functions in Tissue Engineering. *Biomater Sci* **2020**, *8*, 7033–7081.
28. Naahidi, S.; Jafari, M.; Logan, M.; Wang, Y.; Yuan, Y.; Bae, H.; Dixon, B.; Chen, P. Biocompatibility of Hydrogel-Based Scaffolds for Tissue Engineering Applications. *Biotechnol Adv* **2017**, *35*, 530–544.
29. García-González, C.A.; Alnaief, M.; Smirnova, I. Polysaccharide-Based Aerogels - Promising Biodegradable Carriers for Drug Delivery Systems. *Carbohydr Polym* **2011**, *86*, 1425–1438.
30. Baranwal, J.; Barse, B.; Fais, A.; Delogu, G.L.; Kumar, A. Biopolymer: A Sustainable Material for Food and Medical Applications. *Polymers (Basel)* **2022**, *14*.
31. Faulk, D.M.; Londono, R.; Wolf, M.T.; Ranallo, C.A.; Carruthers, C.A.; Wildemann, J.D.; Dearth, C.L.; Badylak, S.F. ECM Hydrogel Coating Mitigates the Chronic

- Inflammatory Response to Polypropylene Mesh. *Biomaterials* **2014**, *35*, 8585–8595, doi:10.1016/j.biomaterials.2014.06.057.
32. Hou, C.; Chen, L.; Yang, L.; Ji, X. An Insight into Anti-Inflammatory Effects of Natural Polysaccharides. *Int J Biol Macromol* **2020**, *153*, 248–255.
33. Teodorescu, M.; Bercea, M.; Morariu, S. Biomaterials of Poly(Vinyl Alcohol) and Natural Polymers. *Polymer Reviews* **2018**, *58*, 247–287.
34. Aydin, A.A.; Ilberg, V. Effect of Different Polyol-Based Plasticizers on Thermal Properties of Polyvinyl Alcohol:Starch Blends. *Carbohydr Polym* **2016**, *136*, 441–448, doi:10.1016/j.carbpol.2015.08.093.
35. Teodorescu, M.; Bercea, M.; Morariu, S. Biomaterials of Poly(Vinyl Alcohol) and Natural Polymers. *Polymer Reviews* **2018**, *58*, 247–287.
36. Tan, J.; Luo, Y.; Guo, Y.; Zhou, Y.; Liao, X.; Li, D.; Lai, X.; Liu, Y. Development of Alginate-Based Hydrogels: Crosslinking Strategies and Biomedical Applications. *Int J Biol Macromol* **2023**, *239*, 124275, doi:https://doi.org/10.1016/j.ijbiomac.2023.124275.
37. Ichimura, K. Photocrosslinkable Poly(Vinyl Alcohols): Preparation Properties and Applications. *Heterogeneous Chemistry Reviews* **1996**, *3*, 419–441, doi:10.1002/(SICI)1234-985X(199612)3:4<419::AID-HCR69>3.0.CO;2-J.
38. Bai, H.; Chen, D.; Zhu, H.; Zhang, S.; Wang, W.; Ma, P.; Dong, W. Photo-Crosslinking Ionic Conductive PVA-SbQ/FeCl₃ Hydrogel Sensors. *Colloids Surf A Physicochem Eng Asp* **2022**, *648*, 129205, doi:https://doi.org/10.1016/j.colsurfa.2022.129205.
39. Bai, H.; Sun, Y.; Xu, J.; Dong, W.; Liu, X. Rheological and Structural Characterization of HA/PVA-SbQ Composites Film-Forming Solutions and Resulting Films as Affected by UV Irradiation Time. *Carbohydr Polym* **2015**, *115*, 422–431, doi:10.1016/j.carbpol.2014.08.103.
40. Ichimura, K.; Watanabe, S. *Preparation and Characteristics of Photocross-Linkable Poly(Vinyl Alcohol)*;
41. Van De Velde, K.; Kiekens, P. *Material Properties Biopolymers: Overview of Several Properties and Consequences on Their Applications*; 2002; Vol. 21;.
42. Alvarado-Hidalgo, F.; Ramírez-Sánchez, K.; Starbird-Perez, R. Smart Porous Multi-Stimulus Polysaccharide-Based Biomaterials for Tissue Engineering. *Molecules* **2020**, *25*.
43. Starbird, R.; García-González, C.A.; Smirnova, I.; Krautschneider, W.H.; Bauhofer, W. Synthesis of an Organic Conductive Porous Material Using Starch Aerogels as Template for Chronic Invasive Electrodes. *Materials Science and Engineering C* **2014**, *37*, 177–183, doi:10.1016/j.msec.2013.12.032.
44. Rodríguez-Quesada, L.; Ramírez-Sánchez, K.; León-Carvajal, S.; Sáenz-Arce, G.; Vásquez-Sancho, F.; Avendaño-Soto, E.; Montero-Rodríguez, J.J.; Starbird-Perez, R. Evaluating the Effect of Iron(III) in the Preparation of a Conductive Porous Composite Using a Biomass Waste-Based Starch Template. *Polymers (Basel)* **2023**, *15*, 2560, doi:10.3390/polym15112560.
45. Santos-Rosales, V.; Alvarez-Rivera, G.; Hillgärtner, M.; Cifuentes, A.; Itskov, M.; García-González, C.A.; Rege, A. Stability Studies of Starch Aerogel Formulations for Biomedical Applications. *Biomacromolecules* **2020**, *21*, 5336–5344, doi:10.1021/acs.biomac.0c01414.

- 1
2
3 46. Beaussart, A.; El-Kirat-Chatel, S.; Sullan, R.M.A.; Alsteens, D.; Herman, P.;
4 Derclaye, S.; Dufrêne, Y.F. Quantifying the Forces Guiding Microbial Cell
5 Adhesion Using Single-Cell Force Spectroscopy. *Nat Protoc* **2014**, *9*, 1049–1055,
6 doi:10.1038/nprot.2014.066.
7
8 47. Zou, F.; Budtova, T. Tailoring the Morphology and Properties of Starch Aerogels
9 and Cryogels via Starch Source and Process Parameter. *Carbohydr Polym* **2021**, *255*,
10 doi:10.1016/j.carbpol.2020.117344.
11
12 48. García-González, C.A.; Concheiro, A.; Alvarez-Lorenzo, C. Processing of Materials
13 for Regenerative Medicine Using Supercritical Fluid Technology. *Bioconjug Chem*
14 **2015**, *26*, 1159–1171, doi:10.1021/bc5005922.
15
16 49. Gurikov, P.; Smirnova, I. Non-Conventional Methods for Gelation of Alginate. *Gels*
17 **2018**, *4*.
18
19 50. Nita, L.E.; Ghilan, A.; Rusu, A.G.; Neamtu, I.; Chiriac, A.P. New Trends in Bio-
20 Based Aerogels. *Pharmaceutics* **2020**, *12*.
21
22 51. Rodríguez-Dorado, R.; López-Iglesias, C.; García-González, C.A.; Auriemma, G.;
23 Aquino, R.P.; Del Gaudio, P. Design of Aerogels, Cryogels and Xerogels of
24 Alginate: Effect of Molecular Weight, Gelation Conditions and Drying Method on
25 Particles' Micromeritics. *Molecules* **2019**, *24*, doi:10.3390/molecules24061049.
26
27 52. Zamora-Sequeira, R.; Ardao, I.; Starbird, R.; García-González, C.A. Conductive
28 Nanostructured Materials Based on Poly-(3,4-Ethylenedioxythiophene) (PEDOT)
29 and Starch/ κ -Carrageenan for Biomedical Applications. *Carbohydr Polym* **2018**,
30 *189*, 304–312, doi:10.1016/j.carbpol.2018.02.040.
31
32 53. Oladzadabbasabadi, N.; Ebadi, S.; Mohammadi Nafchi, A.; Karim, A.A.;
33 Kiahosseini, S.R. Functional Properties of Dually Modified Sago Starch/ κ -
34 Carrageenan Films: An Alternative to Gelatin in Pharmaceutical Capsules.
35 *Carbohydr Polym* **2017**, *160*, 43–51, doi:10.1016/j.carbpol.2016.12.042.
36
37 54. Zhou, T.; Cheng, X.; Pan, Y.; Li, C.; Gong, L. Mechanical Performance and Thermal
38 Stability of Polyvinyl Alcohol–Cellulose Aerogels by Freeze Drying. *Cellulose*
39 **2019**, *26*, 1747–1755, doi:10.1007/s10570-018-2179-3.
40
41 55. Ohta, Y.; Ebisuno, T.; Hasegawa, M. *Dynamic Viscoelastic Properties of Polyvinyl*
42 *with Pendent Styrylpyridinium Alcohol*; 1997; Vol. 2;.
43
44 56. Frost, K.; Kaminski, D.; Kirwan, G.; Lascaris, E.; Shanks, R. Crystallinity and
45 Structure of Starch Using Wide Angle X-Ray Scattering. *Carbohydr Polym* **2009**,
46 *78*, 543–548, doi:10.1016/j.carbpol.2009.05.018.
47
48 57. Kara, S.; Tamerler, C.; Bermek, H.; Nder Pekcan, " Cation Effects on Sol/Gel and
49 Gel/Sol Phase Transitions of κ -Carrageenan/ Water System. *Biological*
50 *Macromolecules* **2022**, *31*, 177–185.
51
52 58. Lascombes, C.; Agoda-Tandjawa, G.; Boulenguer, P.; Le Garnec, C.; Gilles, M.;
53 Mauduit, S.; Barey, P.; Langendorff, V. Starch-Carrageenan Interactions in Aqueous
54 Media: Role of Each Polysaccharide Chemical and Macromolecular Characteristics.
55 *Food Hydrocoll* **2017**, *66*, 176–189, doi:10.1016/j.foodhyd.2016.11.025.
56
57 59. Kahvand, F.; Fasihi, M. Plasticizing and Anti-Plasticizing Effects of Polyvinyl
58 Alcohol in Blend with Thermoplastic Starch. *Int J Biol Macromol* **2019**, *140*, 775–
59 781, doi:10.1016/j.ijbiomac.2019.08.185.
60
60. Aydin, A.A.; Ilberg, V. Effect of Different Polyol-Based Plasticizers on Thermal
Properties of Polyvinyl Alcohol:Starch Blends. *Carbohydr Polym* **2016**, *136*, 441–
448, doi:10.1016/j.carbpol.2015.08.093.

- 1
2
3 61. Luo, X.; Li, J.; Lin, X. Effect of Gelatinization and Additives on Morphology and
4 Thermal Behavior of Corn Starch/PVA Blend Films. *Carbohydr Polym* **2012**, *90*,
5 1595–1600, doi:10.1016/j.carbpol.2012.07.036.
6
7 62. Sin, L.T.; Rahmat, A.R.; Rahman, W.A.W.A.; Sun, Z.Y.; Samad, A.A. Rheology
8 and Thermal Transition State of Polyvinyl Alcohol-Cassava Starch Blends.
9 *Carbohydr Polym* **2010**, *81*, 737–739, doi:10.1016/j.carbpol.2010.03.044.
10
11 63. Croitoru, C.; Pop, M.A.; Bedo, T.; Cosnita, M.; Roata, I.C.; Hulka, I. Physically
12 Crosslinked Poly (Vinyl Alcohol)/Kappa-Carrageenan Hydrogels: Structure and
13 Applications. *Polymers (Basel)* **2020**, *12*, doi:10.3390/polym12030560.
14
15 64. Masanabo, M.A.; Ray, S.S.; Emmambux, M.N. Properties of Thermoplastic Maize
16 Starch-Zein Composite Films Prepared by Extrusion Process under Alkaline
17 Conditions. *Int J Biol Macromol* **2022**, *208*, 443–452,
18 doi:https://doi.org/10.1016/j.ijbiomac.2022.03.060.
19
20 65. Rwei, S.-P.; Chen, S.-W.; Mao, C.-F.; Fang, H.-W. Viscoelasticity and Wearability
21 of Hyaluronate Solutions. *Biochem Eng J* **2008**, *40*, 211–217,
22 doi:https://doi.org/10.1016/j.bej.2007.12.021.
23
24 66. Ichimura, K. Photocrosslinkable Poly(Vinyl Alcohols): Preparation Properties and
25 Applications. *Heterogeneous Chemistry Reviews* **1996**, *3*, 419–441,
26 doi:10.1002/(SICI)1234-985X(199612)3:4<419::AID-HCR69>3.0.CO;2-J.
27
28 67. Vega-Rios, A.; Olmedo-Martínez, J.L.; Farías-Mancilla, B.; Hernández-Escobar,
29 C.A.; Zaragoza-Contreras, E.A. Synthesis and Electrical Properties of
30 Polyaniline/Iota-Carrageenan Biocomposites. *Carbohydr Polym* **2014**, *110*, 78–86,
31 doi:https://doi.org/10.1016/j.carbpol.2014.03.068.
32
33 68. Diah, A.W.M.; Saehana, S.; Holdsworth, C.I. Potency of Carrageenan as the Doping
34 Agent for Poly(3,4-Ethylenedioxythiophene) Conductive Polymer. In Proceedings of
35 the Journal of Physics: Conference Series; Institute of Physics Publishing, July 1
36 2019; Vol. 1242.
37
38 69. Pérez-Madrigal, M.M.; Estrany, F.; Armelin, E.; Díaz, D.D.; Alemán, C. Towards
39 Sustainable Solid-State Supercapacitors: Electroactive Conducting Polymers
40 Combined with Biohydrogels. *J Mater Chem A Mater* **2016**, *4*, 1792–1805,
41 doi:10.1039/c5ta08680a.
42
43 70. Padhi, A.; Nain, A.S. ECM in Differentiation: A Review of Matrix Structure,
44 Composition and Mechanical Properties. *Ann Biomed Eng* **2020**, *48*, 1071–1089.
45
46 71. Lu, Y.; Wang, W. Interaction between the Interstitial Fluid and the Extracellular
47 Matrix in Confined Indentation. *J Biomech Eng* **2008**, *130*, doi:10.1115/1.2939310.
48
49 72. Akhtar, R.; Sherratt, M.J.; Cruickshank, J.K.; Derby, B. Characterizing the Elastic
50 Properties of Tissues. *Materials Today* **2011**, *14*, 96–105.
51
52 73. Lin, D.C.; Horkay, F. Nanomechanics of Polymer Gels and Biological Tissues: A
53 Critical Review of Analytical Approaches in the Hertzian Regime and Beyond. *Soft
54 Matter* **2008**, *4*, 669–682, doi:10.1039/b714637j.
55
56 74. Padhi, A.; Nain, A.S. ECM in Differentiation: A Review of Matrix Structure,
57 Composition and Mechanical Properties. *Ann Biomed Eng* **2020**, *48*, 1071–1089.
58
59 75. Taylor, Z.; Miller, K. Reassessment of Brain Elasticity for Analysis of
60 Biomechanisms of Hydrocephalus. *J Biomech* **2004**, *37*, 1263–1269,
doi:10.1016/j.jbiomech.2003.11.027.
76. Soza, G.; Grosso, R.; Nimsky, C.; Hastreiter, P.; Fahlbusch, R.; Greiner, G.
Determination of the Elasticity Parameters of Brain Tissue with Combined

- 1
2
3 Simulation and Registration. *International Journal of Medical Robotics and*
4 *Computer Assisted Surgery* **2005**, *01*, 87, doi:10.1581/mrcas.2005.010308.
5 77. Zhu, J.; Sabharwal, T.; Kalyanasundaram, A.; Guo, L.; Wang, G. Topographic
6 Mapping and Compression Elasticity Analysis of Skinned Cardiac Muscle Fibers in
7 Vitro with Atomic Force Microscopy and Nanoindentation. *J Biomech* **2009**, *42*,
8 2143–2150, doi:10.1016/j.jbiomech.2009.05.031.
9 78. Turner, C.H.; Rho, J.; Takano, Y.; Tsui, T.Y.; Pharr, G.M. *The Elastic Properties of*
10 *Trabecular and Cortical Bone Tissues Are Similar: Results from Two Microscopic*
11 *Measurement Techniques*; 1999; Vol. 32;.